ADVANCED FUNCTIONAL MATERIALS

FULL PAPER

DOI: 10.1002/adfm.200600825

# Nanostructure-Dependent Vertical Charge Transport in MEH-PPV Films**

By *Yi-Fang Huang*, *Anto R. Inigo*, *Chia-Chen Chang*, *Kang-Chuang Li*, *Chiao-Fan Liang*, *Chan-Wei Chang*, *Tsong-Shin Lim*, *Su-Hua Chen*,* *Jonathon David White*,* *U-Ser Jeng*,* *An-Chung Su*,* *Ying-Sheng Huang*, *Kang-Yung Peng*, *Show-An Chen*, *Woei-Wu Pai*,* *Chen-Hong Lin*, *Alexey R. Tameev*, *Sergey V. Novikov*, *Anatoly V. Vannikov*, and *Wun-Shain Fann**

The correlation between morphology and charge-carrier mobility in the vertical direction in thin films of poly(2-methoxy-5-(2′-ethylhexyloxy)-1,4-phenylenevinylene) (MEH-PPV) is investigated by a combination of X-ray reflectivity (XRR), field-emission scanning electron microscopy (FESEM), atomic force microscopy (AFM), fluorescence optical microscopy (FOM), photoluminescence spectroscopy (PL), photoluminescence excitation spectroscopy (PLE), as well as time-of-flight (TOF) and transient electroluminescence (TrEL) techniques. The mobility is about two orders of magnitude greater for drop-cast films than for their spin-cast counterparts. Drop-casting in the presence of a vertical static electric field (E-casting) results in films with an additional increase in mobility of about one order of magnitude. While PL and PLE spectra vary with the method of film preparation, there is no correlation between emission spectra and charge-carrier mobility. Our XRR measurements on spin-cast films indicate layering along the film depth while no such structure is found in drop-cast or E-cast films, whereas FESEM examination indicates that nanodomains within drop-cast films are eliminated in the E-cast case. These observations indicate that carrier transport is influenced by structure on two different length scales. The low mobility observed in spin-cast films is a direct result of a global layered structure with characteristic thickness of ca. 4 nm: in the absence of this layered structure, drop-cast films with inherent nanoscale heterogeneities (ca. 20 nm in size) exhibit much better hole mobility. Elimination of nanodomains via electric-field alignment results in further improved charge mobility.

## 1. Introduction

Polymers with conjugated π-electrons along the backbone play an important role in organic electronic applications because of their unique mechanical and electronic properties.[1–3] Although the extended π–π conjugation has been the main point of focus, it is more generally the van der Waals interac-

[*] Prof. W. S. Fann, Dr. Y. F. Huang, Dr. A. R. Inigo, C. C. Chang, K. C. Li, C. F. Liang, C. W. Chang, Dr. T. S. Lim
Institute of Atomic and Molecular Sciences, Academia Sinica
P. O. Box 23–166, Taipei 106 (Taiwan)
Prof. W. S. Fann, Dr. Y. F. Huang, Dr. A. R. Inigo, C. C. Chang, K. C. Li, C. F. Liang, C. W. Chang, Dr. T. S. Lim
Department of Physics and Institute of Polymer Science and Engineering, National Taiwan University, Taipei 106 (Taiwan)
E-mail: fann@gate.sinica.edu.tw
Prof. S. H. Chen
Department of Materials Science and Engineering
National Dong Hwa University
Hualien 974 (Taiwan)
E-mail: shchen@mail.ndhu.edu.tw
Prof. J. D. White
Department of Electrical Engineering, Yuan Ze University
Neili, Taoyuan 320 (Taiwan)
E-mail: whitejd@yiaotu.com
Dr. U S. Jeng
National Synchrotron Radiation Research Center
Hsinchu 300 (Taiwan)
E-mail: usjeng@nsrrc.org.tw
Prof. A. C. Su, Dr. K. Y. Peng, Prof. S. A. Chen
Department of Chemical Engineering, National Tsing Hua University
Hsinchu 300 (Taiwan)
Prof. A. C. Su
Institute of Materials Science and Engineering
National Sun Yat-sen University
Kaohsiung 804 (Taiwan)
E-mail: acsu@mx.nthu.edu.tw
Prof. Y. S. Huang
Department of Electronic Engineering
National Taiwan University of Science and Technology
Taipei 106 (Taiwan)
Prof. W. W. Pai, C. H. Lin
Center for Condensed Matter Sciences, National Taiwan University
Taipei 106 (Taiwan)
E-mail: wpai@ntu.edu.tw
Dr. A. R. Tameev, Dr. S. V. Novikov, Prof. A. V. Vannikov
A. Frumkin Institute of Physical Chemistry and Electrochemistry of RAS
Moscow 119991 (Russia)

[**] This work is financially supported by the National Science Council under contract numbers NSC95-2752-E-007-007-PAE (Program for Prompting Academic Excellence in Universities), NSC93-2120 M-002-009, and 94WIA0100022 (NSC-RFBR Joint Research Project). X-ray reflectivity measurements were made at Beamline 17B of the NSRRC. A.R.T., S.V.N., and A.V.V. are grateful to the Russian Foundation for Basic Research for support under the RFBR project 05-03-90579-HHC. We also thank S. S. Huang for technical help. Supporting information is available online from Wiley InterScience or from the author.


WILEY InterScience DISCOVER SOMETHING GREAT

© 2007 WILEY-VCH Verlag GmbH & Co. KGaA, Weinheim

ADVANCED FUNCTIONAL MATERIALS



tions between polymer chains (as well as those between polymer and solvent molecules in solution-processed films) that determine the ways of chain packing in the film state. This in turn exerts significant effects on chain conformation/aggregation, backbone co-planarity, and hence on the electronic properties.[4,5] Extensive studies have shown that the electronic properties of conjugated polymers may depend on the film-processing conditions, such as the solvent used, the solution concentration, and methods/conditions of film preparation.[6] On the whole, the fact that the film morphology developed during processing bears a significant effect on the device performance is well-established.[7] While the operation of devices, such as light-emitting diodes, solar cells, and field-effect transistors, involves various factors, charge-carrier transport is one of the most important and yet least understood properties. Thus, there is a need to establish the correlation between processing methods, morphological characteristics, and resulting charge-transport behavior.

Numerous spectroscopic investigations have been made on a variety of solutions and thin films of poly(2-methoxy-5-(2′-ethylhexyloxy)-1,4-phenylenevinylene) (MEH-PPV, the most studied model for semiconducting polymers), addressing the effects of inter-chain interactions on the photophysical properties.[8] It is generally concluded that packing of MEH-PPV chains in the aggregated state affects the chain conformation and conjugation length, and, thus, the optical properties. While a positive correlation between inter-chain interaction and charge-carrier transport has been speculated,[8] the issue has not been subjected to extensive experimental scrutiny as has its photophysical counterpart. In order to study the effects of structure on charge mobility, various methods were used to prepare films of differing structural heterogeneity. Drop-casting was used to prepare films that are in quasi-thermal equilibrium, that is, the slow solvent-evaporation method gives polymers time to relax to their lowest energy states. Spin-coating was used to prepare films whose structure is process-dominated, in other words, it is dictated by the centrifugal forces and rapid solvent evaporation involved in the spin-casting process. Drop-casting in the presence of a static electric field (previously observed to inhibit domain formation)[9] was used to produce films in a perturbed thermal-equilibrium state. Our results indicate that the carrier mobility in MEH-PPV films depends clearly on the different levels of structural heterogeneity developed along the charge-transport path. In addition to inter-chain interactions (indicated by optical evidence), the nature of domain structures and their orientation relative to the transport direction play a dominant role in the charge-transport behavior.

## 2. Results

### 2.1. Optical and Topographic Measurements

The films were first checked using fluorescent confocal microscopy and atomic force microscopy (AFM). A typical fluorescence image is shown in Figure 1. All the films investigated (whether drop-cast, spin-cast, or drop-cast in the presence of an electric field, denoted hereafter as E-cast) exhibited a similar optical homogeneity over the film surface, demonstrating that the films are of good quality and optically homogeneous over a broad area. This was confirmed by AFM (Fig. 2) on the micrometer-scale, where the root-mean-square

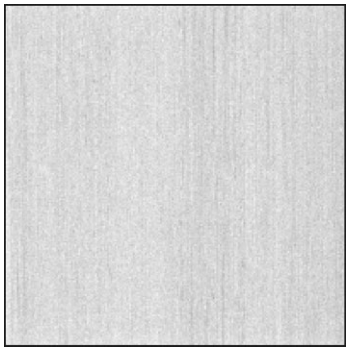

**Figure 1.** Fluorescence image of drop-cast (ca. 4.0 μm in thickness) MEH-PPV film. The scanned area was 40 μm × 40 μm, excitation wavelength was $\lambda_{exc}$ = 460 nm, and fluorescence wavelengths beyond 515 nm were used for imaging. Both excitation and detection bandwidths were chosen for maximized signal-to-noise ratio.

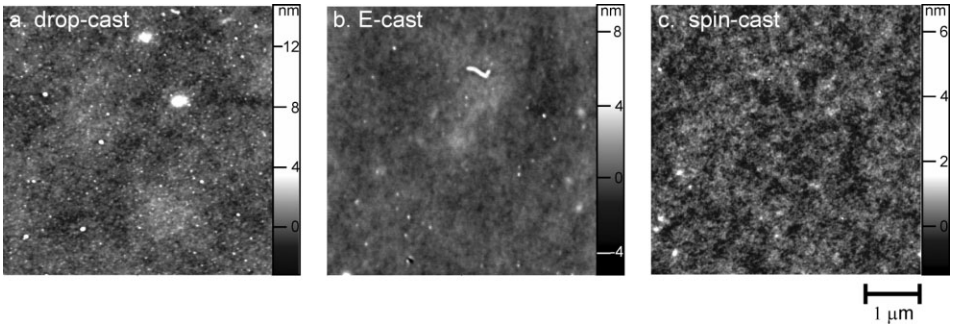


**Figure 2.** Topographic images taken by AFM of a) drop-cast (4.0 μm in thickness), b) E-cast (3.7 μm), and c) spin-cast (22 nm) MEH-PPV films shown in Figure 1. Drop-cast and spin-cast films are deposited directly on glass while the E-cast film is deposited on ITO-coated glass (a slightly rougher substrate). Values of root-mean-square surface roughness over the 5 μm × 5 μm scan area were 0.77 nm, 0.60 nm, and 0.36 nm for drop-cast, E-cast, and spin-cast films, respectively.


© 2007 WILEY-VCH Verlag GmbH & Co. KGaA, Weinheim

surface roughness over the 25 $\mu m^2$ scanned area is less than 1 nm in all cases.

The photoluminescence (PL) and photoluminescence excitation (PLE) spectra of drop-cast, E-cast, and spin-cast devices are shown in Figure 3. The peak at ca. 640 nm in the PL spectra is indicative of the relative amount of inter-chain interaction present in the different polymer films.[8,10–12] The higher intensity around 640 nm in the drop-cast film (Fig. 3a) indicates that this specimen has the highest concentration of the red-light-emitting species which is attributed to the inter-chain interactions. Similar information can be inferred from the PLE spectra (Fig. 3b).[8,10] The progressively red-shifted edge from spin-cast, E-cast, to drop-cast specimens indicates more extended conjugation in the latter cases. In other words, the inter-chain species is more abundant in drop-cast and E-cast films than in spin-cast films with the amount of inter-chain species being highest in the drop-cast film. We note that a similar difference in the PL spectra between drop- and spin-cast MEH-PPV films prepared from a toluene solution has been reported.[13]

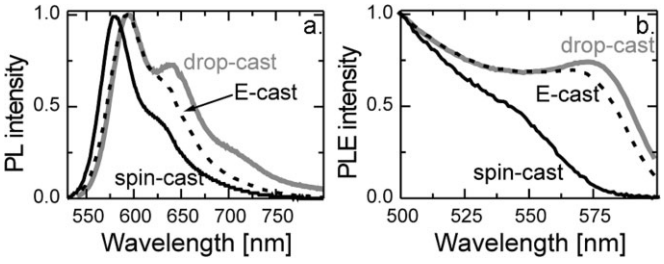


**Figure 3.** a) Photoluminescence (excited at 510 nm) and b) photoluminescence excitation spectra (monitored at 630 nm) of drop-cast, E-cast, and spin-cast films.

Time-resolved PL is a third method to probe the inter-chain interactions in MEH-PPV films.[8] If the amount of inter-chain species increases, the difference between the decay curves monitored at the peak (590 nm for drop-cast films and 580 nm for spin-cast films) and at the shoulder (630 nm for drop-cast, 620 nm for spin-cast films) will also increase because of the increased energy transfer from intra-chain species to inter-chain (red-light-emitting) species. Figure 4 shows the time-resolved PL decay curves monitored at the peak and shoulder of each film. Note that all curves have been peak normalized to unity. While there is a considerable difference between the two curves for the drop-cast film, they are nearly identical in the spin-cast case. The film that was drop-cast in the presence of an electric field lies somewhere in the middle. This indicates that the concentration of inter-chain species is highest in the drop-cast film. The nearly identical curves in the spin-cast case indicate that there is only one emission species (intra-chain species) in the spin-cast film.

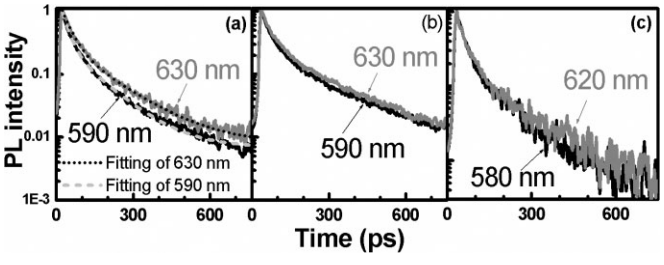


**Figure 4.** Time-resolved photoluminescence spectra of a) drop-cast, b) E-cast, and c) spin-cast MEH-PPV films. The dotted- and dashed-lines in (a) are the fitting (using two exponential) results of a drop-cast film monitored at 630 nm (with decay time of 35 ps and 150 ps, $\chi^2 = 0.99830$) and 590 nm (with decay time of 30 ps and 120 ps, $\chi^2 = 0.99884$), respectively.

To summarize, our PL, PLE, and corresponding time-resolved measurements all indicate that the concentration of the inter-chain species is highest in drop-cast films and lowest in spin-cast films. While the PL spectral differences are open to different interpretations (i.e., increased self-absorption in the thicker films may possibly be related to scattering from domains within these films), the PLE and time-resolved measurements provide unambiguous support for the previous conclusion. We note that the collapse of MEH-PPV chains into the inter-chain species requires time. In the spin-coating process, rapid solvent evaporation and stresses induced in the process should inhibit this collapse. On the other hand, the existence of an external electric field clearly affects the energy equilibrium thus suppressing the formation of the inter-chain species as seen in Figure 3.

### 2.2. Charge-Carrier Mobility

The mobility was measured using the time-of-flight (TOF) technique for thick films and transient electroluminescence (TrEL) for thin films. Although it would be preferable to have charge mobility in different films determined using the same measurement method, it is fundamentally inappropriate to use the TOF method for spin-coated films since for TOF the charge-carrier sheet should be thin compared to the film thickness. In the case of MEH-PPV, the optical penetration depth is about 100 nm. While this is considerably less than the thickness (4 μm) of drop-cast and E-cast films, this is not the case for the spin-cast film, which was only 22 nm in thickness. Thus, it was necessary to use different techniques for the mobility measurements. As a result, extra care must be taken in comparing the carrier-mobility values obtained for spin-cast and drop-cast films. In addition, there are considerable uncertainties in the value of mobility obtained by the TrEL method because of the following reasons. Our TrEL measurements involve the superposition of hole transport towards the Al cathode and interfacial charging at the cathode, followed by enhanced electron injection and electron–hole recombination within the MEH-PPV layer. In order to ensure that mobility was hole dominated, an Al cathode was used for both TOF and TrEL measurements. While ensuring hole dominance, the Al cathode limits the rate of electron injection. Accumulated charges may then lead to increased delay times. Thus, the mobility values determined from the measured delay times correspond to lower estimates. Based on a theoretical approach[14] describing an analogous influence of the injection barrier in bi-layer organic light-emitting diodes (OLEDs), we estimate that the hole mobility mea-


© 2007 WILEY-VCH Verlag GmbH & Co. KGaA, Weinheim

ADVANCED FUNCTIONAL MATERIALS



sured for our spin-cast films could be underestimated by as much as an order of magnitude.

Figure 5 presents TOF data for drop-cast and E-cast devices at an applied electric field of $E = 88\ \mathrm{kV\,cm^{-1}}$. The initial spike is due to the capacitance of the device. The transit time was determined from the kink in the corresponding logarithmic plot. The transit time for the holes in the E-cast device is an order of magnitude shorter than that in the drop-cast device, resulting in an order of magnitude difference in mobility ($\mu_d$). In the case of the drop-cast device, $\mu_d = 2.2 \times 10^{-6}\ \mathrm{cm^2\,V^{-1}\,s^{-1}}$ whereas for the E-cast device $\mu_d = 1 \times 10^{-5}\ \mathrm{cm^2\,V^{-1}\,s^{-1}}$. We note that in the E-cast device the appearance of a cusp serves as a signature of a memory effect involving injected charges and is indicative of strongly non-dispersive hole transport. A full discussion of the cusp and its significance has been given by Bässler and coworkers.[15] Figure 6 shows TrEL data for the spin-cast film at applied voltages of 12 V ($E = 4000\ \mathrm{kV\,cm^{-1}}$) and 18 V ($E = 6000\ \mathrm{kV\,cm^{-1}}$) in both logarithmic and linear scales. As the applied voltage increases, the delay time decreases, reflecting an increase in charge-carrier mobility. The transit and delay times, respectively, were derived from the corresponding logarithmic TOF and TrEL profiles.

Figure 7 summarizes and compares the field-dependent mobility of drop-cast, E-cast, and spin-cast devices plotted as a function of the square root of the applied electric field. The mobility of the E-cast device is consistently over two orders of magnitude higher than that of the spin-cast device and one order of magnitude higher than that of the drop-cast device.

### 2.3. Film Morphology

The film structure was further investigated using X-ray reflectivity (XRR) and field-emission scanning electron microscopy (FESEM). Figure 8 shows the XRR profiles measured in the out-of-plane direction for the drop-cast, E-cast, and spin-cast films. Profiles of the thicker drop-cast and E-cast films are relatively featureless, indicating film homogeneity. In contrast, considerable structure is seen for the spin-cast film. This film's profile is characterized by high-frequency fringes ($\Delta Q' = 0.028\ \mathrm{Å^{-1}}$) modulated at $\Delta Q = 0.15\ \mathrm{Å^{-1}}$. The former ($\Delta Q'$), identified as Kiessig fringes, indicate that the film is of good optical quality with a thickness $t = 2\pi/\Delta Q' = 22$ nm. The

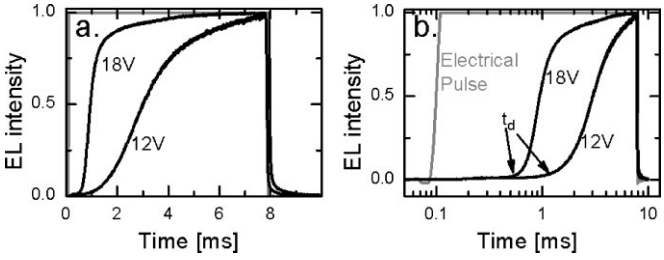


**Figure 6.** Transient electroluminescence (TrEL) signals for the spin-cast device at applied voltages of 12 V and 18 V, in a) linear and b) semi-logarithmic scales. Applied voltage pulses are shown in grey.

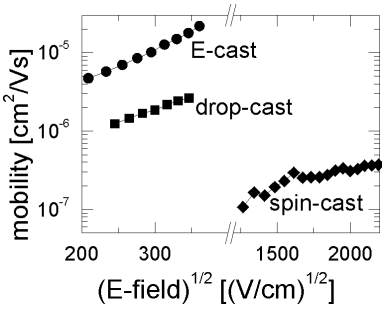


**Figure 7.** Comparison among room-temperature field-dependent mobility for drop-cast, E-cast, and spin-cast devices. Mobility in the spin-cast film may have been underestimated (see text).

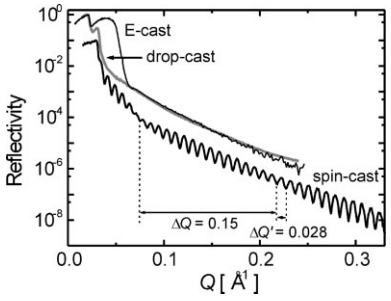


**Figure 8.** X-ray reflectivity profiles of drop-cast, E-cast, and spin-cast MEH-PPV films from chlorobenzene solutions, where $\Delta Q'$ is the period of Kiessig fringes whereas $\Delta Q$ is the period of amplitude modulation in Kiessig fringes.

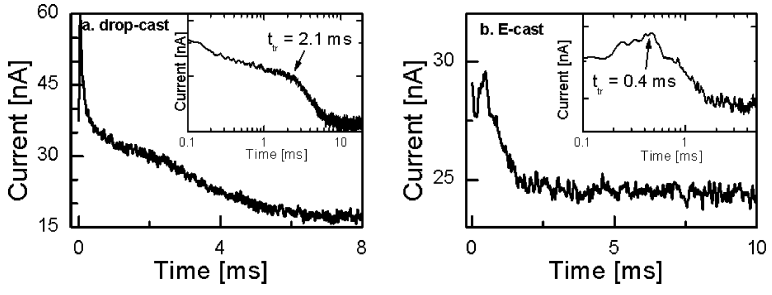


**Figure 5.** Time-of-flight (TOF) signal for a) drop-cast and b) E-cast devices at an applied electric field of $E = 8.8 \times 10^4\ \mathrm{V\,cm^{-1}}$. Given as insets are corresponding logarithmic plots.

latter, resulting from alternating sub-layers of high and low electron densities, indicates global layering along the film depth with characteristic spacing $t_{layer} = 2\pi/\Delta Q = 4.2$ nm. Note that this layered structure, being parallel to the surface, does not give any contrast in plane-view fluorescence microscopy (FOM) or AFM.

To clarify whether this layered structure is generic to the spin-casting process or a consequence of self-organizing characteristics of MEH-PPV in the thin-film state, a number of checks were performed. Firstly, films of thicknesses ranging from 22 to 203 nm (varied by controlling the spin speed) were

 © 2007 WILEY-VCH Verlag GmbH & Co. KGaA, Weinheim 

spin-cast and their XRR profiles obtained (Fig. S2, Supporting information). In all cases, both Kiessig fringes and their modulations are clearly visible although the global layer spacing increases by a factor of 2 ($t_{layer} = 4.2$ to 9.0 nm) as the thickness increases by a factor of 9 ($t = 22$ to 203 nm). This means that global layering is not directly related to the bilayer stacking discussed in previous reports.[16,17] Secondly, thinner films (3.5 and 2.6 μm in thickness) were drop-cast to see if global layering may emerge with decreasing film thickness. Corresponding XRR profiles of these thinner films (Fig. S3) are basically featureless, indicating homogeneity in the thickness direction. In fact, the XRR profiles are well described by Fresnel curves corresponding to uniform films sitting on the indium tin oxide (ITO) glass substrate (i.e., absence of layering). It is therefore clear that the global layering is generic to the spin-casting process.

As XRR profiles for drop-cast and E-cast films indicate an absence of global layering, the morphology of these two types of films was investigated via FESEM. Figure 9 compares the cross-sectional topographic features of cryogenically fractured drop-cast and E-cast films. Domains on the nanometer scale are clearly seen for the drop-cast film, which are not observable for the E-cast case. This indicates that the E-cast film is more homogeneous than the drop-cast film in real space, which is consistent with the published X-ray measurements made in reciprocal space.[16,18] Attempts to perform similar cross-sectional FESEM observation on the spin-cast film were not successful because of the difficulties in handling the much thinner specimens: debonding and curling inevitably occur in our cryogenic fracture procedure.

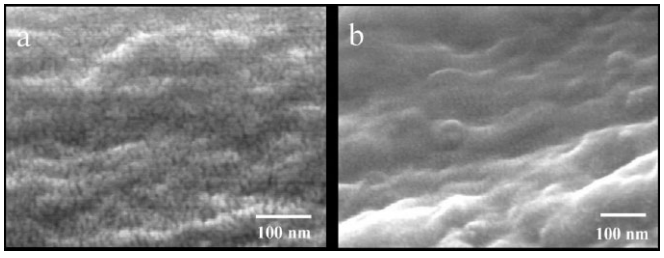


**Figure 9.** Cross-section FESEM images of cryogenically fractured a) drop-cast and b) E-cast MEH-PPV films to expose the interior morphology.

## 3. Discussion

Differences in field-dependent carrier mobility for different films (Fig. 7) can be perplexing if one considers only the optical and the mobility data. For example, comparing the PL spectra of drop-cast and spin-cast films (Fig. 3a), it appears that the higher mobility observed in the drop-cast film (Fig. 6) is due to the relatively higher amount of inter-chain species (increased height of the secondary peak at 640 nm). The fact that the PL spectra of the spin-cast film (Fig. 3a) is blue-shifted by 10 nm relative to the other two films is a further indicator that inter-chain interaction is weaker in the spin-cast device than in the drop-cast case. However, if we continue this line of reasoning, one would then expect to observe a lower mobility in the E-cast film as optical spectroscopy indicates that the inter-chain interactions are weaker than that of drop-casting films. This is clearly not the case. While the mobility in the spin-cast device is one to two orders of magnitude lower than that in the drop-cast device, the mobility in the E-cast device is one order of magnitude higher than that for the drop-cast film. In summary, the optical measurements presented above have demonstrated that the films are uniform on a length scale > 250 nm (limits of resolution of confocal microscopy) whereas charge transport is not directly correlated with optical differences related to features < 10 nm in size (as elucidated by PL measurements). This suggests that morphological features intermediate in size are the key to understanding the charge mobility and it is necessary to take into account the film structure on two different length scales.

On the one hand, PL emission provides information on the local environment. It is primarily related to inter-chain interactions and is basically governed by local structures and energy-transfer routes within these structures. On the other hand, charge transport, while influenced by these structures, is in addition impacted by the existence of structure on a larger length scale as a carrier must travel through the entire film thickness, from one electrode to the other. This larger length scale is not visible from optical spectroscopy. Previous studies, making use of optical spectroscopy, atomic force microscopy, and X-ray diffraction, have extensively investigated the local environment responsible for PL emission. In these studies, drop-cast MEH-PPV films have been shown to comprise nanometer-sized domains of different orientations.[16–18] Such nanodomains are clearly discernible in Figure 9a but not in Figure 9b. Structural analysis has shown that mobility is related to the orientation of these domains.[19] As seen in Figure 9b, application of an electric field during drop-casting tends to eliminate these domains, which is consistent with the spectra in Figure 3. This elimination of nanodomains results in an increase in the mobility and a decrease of the intensity of the emission peak at 640 nm.[18]

The present XRR results (Fig. 8) indicate the existence of global layering in spin-cast films that is not evident in drop-cast or E-cast films.[20] The layer normal is perpendicular to the substrate and hence lies parallel to the charge-transport direction. Presumably, each layer in the spin-cast film consists of a sublayer of ordered inter-backbone stacking and a sublayer of lower electron density. While spin-cast films have a lower concentration of inter-chain emissive species than drop-cast or E-cast films on the basis of PL and PLE data (Fig. 3), disordered sublayers serve as barriers for charge transport and result in decreased mobility in the spin-cast film.

In commonly accepted models of charge hopping in disordered organic materials, variation of the magnitude of the mobility associated with morphological variation is related to changes in the magnitude of the mobility prefactor ($\mu_0$), energy disorder ($\sigma$), and positional ($E$) disorder.[21] Both energy and positional disorder can be derived from the temperature and field dependence of the carrier mobility. For the drop-cast film they are $\sigma = 86$ meV and $E = 3.6$; for the E-cast film they are $\sigma = 71$ meV and $E < 1.5$;[18] in other words, the energy disorder


© 2007 WILEY-VCH Verlag GmbH & Co. KGaA, Weinheim

ADVANCED FUNCTIONAL MATERIALS



is similar for the two films whereas the positional disorder (reflecting fluctuations in distance and orientation between hopping sites) varies greatly. This is in support of the contention that geometric factors (packing of MEH-PPV units, orientation of domains, etc.) are the major reasons for the variations in carrier mobility. Detailed analysis and discussion on temperature-dependent mobility were reported earlier for the drop- and E-cast devices. Extension to temperature-mobility data for spin-cast films would be interesting, but these are not available as yet.

Our resulting picture of morphology-dependent hole transport in MEH-PPV is summarized in Figure 10. We start by recapitulating the key morphological features. The drop-cast film (slowly dried under quasi-equilibrium conditions) is characterized by a significant volume fraction of ordered domains that are dispersed (in a more-or-less aligned manner) in the amorphous host.[16] Presence of a static electric field perturbs the film formation process, resulting a in decreased volume fraction of ordered domains.[18] The spin-casting process also results in a decreased volume fraction of ordered domains, but these tend to coalesce into layers lying parallel to the film surface. On the basis of the current understanding of charge transport and luminescence properties of MEH-PPV (and conjugated polymers in general), we assume that the ordered domains are characterized by higher *intra*-domain hole mobility. Trapping of holes occurs mainly at domain boundaries when the holes, directed by the electric field, are trying to leave the ordered domains and enter the amorphous matrix.

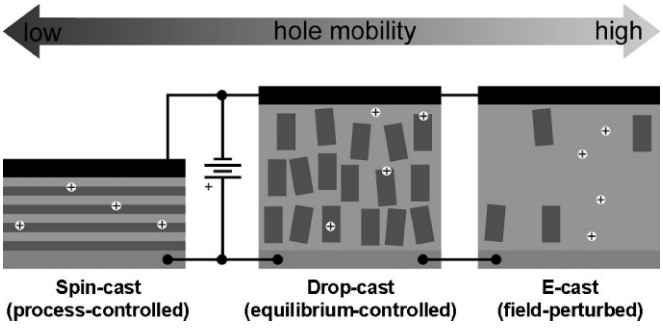


**Figure 10.** Charge-transport paths in ITO/MEH-PPV/Al devices. Ordered domains (dark grey) of high electron density are schematically shown as distributed within the lighter matrix of low electron density. Spatial distribution of ordered and disordered domains determines routes of holes (white crosses) traveling through the film.

In the case of E-cast films, the substantially decreased volume fraction of ordered domains (due to perturbation by the electric field during film formation) means that carriers are unlikely to hit ordered domains; hence they travel at a steady (although admittedly low) velocity through the amorphous matrix. For the drop-cast film, numerous domains are more or less aligned,[16] resulting in preferred paths where carriers move quickly within each ordered domain but then get trapped at the domain boundary; escape from the trapping site is achieved by hopping across the inter-domain gap. Thus holes experience repeated scenarios of fast intra-domain traveling–trapping–hopping, which renders the transport process intermittent and less efficient. The worst mobility case occurs in the spin-cast film: the presence of alternating sub-layers of ordered and amorphous regions renders it necessary for carriers to make long and difficult hops (in the order of 4 nm); transport in the spin-cast film is therefore significantly slowed down by extended dormant periods of carriers trapped at the interface of ordered and amorphous regions. The carrier-transport behavior in these films is thus analogous to the proverbial story of the tortoise and the hare, in which the slow-but-steady wins the race.

With the morphology–mobility relationship discussed, some comments on the processing–morphology relationship are in order. The observed morphological differences likely arise from differences in the casting techniques. In spin-casting, the solvent evaporates quickly, and the speed-dependent shearing force is likely dominant, forcing MEH-PPV to form a streamlined morphology during the laminar flow in spin-casting. In contrast, the drop-cast procedure adopted here involves an atmosphere rich in solvent vapor which slows film formation providing adequate time for nanodomains to nucleate and re-orientate themselves into a more energy favorable configuration. As a consequence, in drop-cast films, nanodomain aggregation of MEH-PPV is preferred over a layer-like structure. As for the E-cast process, chain alignment under a static vertical electric field during solvent evaporation would favor orientational order rather than positional order and hence inhibit nucleation/development of nanodomains. The mechanism allowing for this interaction, however, must be indirect as MEH-PPV is relatively non-polar. We believe this is most likely because of the electric field interacting with the polar chlorobenzene molecules which in turn interact with the MEH-PPV polymer. We have tested this hypothesis by replacing chlorobenzene with toluene, which is less polar. The enhancement in carrier mobility was found to be only a factor of three or less, as also demonstrated by Shi et al.[22] A further check on this interpretation was made by applying an electric field parallel to the substrate (by simply not applying the Ag paste, see Fig. 11a). In this case, there was no enhancement effect. Thus, not only the existence of an electric field but also its direction is important.

While these three methods of depositing films do not exhaust all possible ways of sample preparation, they do demonstrate that there are several levels of complexity in film morphology. Processing affects film morphology from the sub-nanometer to the millimeter scale, which is then reflected in differences in electronic and optical properties of the thin film. Morphological changes on a scale of less than 10 nm result in changes to the films optical properties such as absorption and emission spectra. Morphological changes on a scale of greater than 100 nm will be optically visible, using near-field optics, confocal optics, or with the naked eye. Changes on all length scales affect the charge-transport properties. In this paper, we have highlighted the effects of morphological changes that are optically invisible on charge transport, especially features with length scales greater than 10 nm and less than 100 nm.


© 2007 WILEY-VCH Verlag GmbH & Co. KGaA, Weinheim

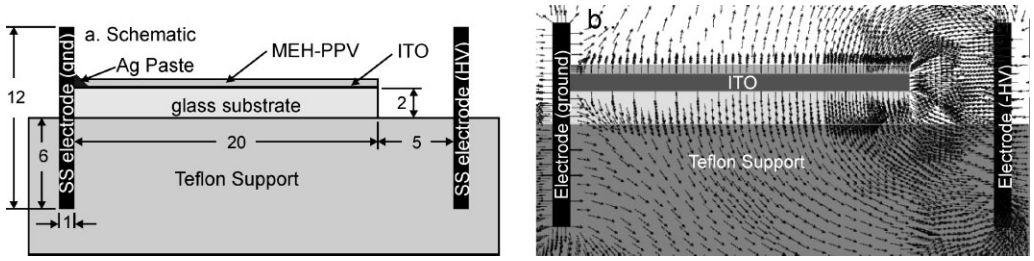


**Figure 11.** a) Cross-section of the experimental setup for the application of the electric field during drop-casting. Dimensions are given in mm. The electrodes extend 50 mm into the page. b) Electric-field distribution around and within the MEH-PPV film. The static electric field within the MEH-PPV layer is essentially along the film normal.

## 4. Conclusions

Mechanisms that determine the optical properties and the charge-carrier mobility are not identical. An enhancement or diminishment of local inter-chain interactions seen in the PL spectrum does not necessarily lead to either higher or lower carrier mobilities (i.e., increasing aggregation does not automatically increase mobility as might be concluded in comparing only drop-cast and spin-cast films). Rather, carrier transport is influenced by the interplay of structures on different length scales. The lower mobility observed in spin-cast films as compared to drop-cast films is a direct result of large-scale layering generic to the spin-casting process. Slow solvent evaporation in our drop-cast films allows for formation of localized nanodomains, which results in higher carrier mobility. Elimination of these nanodomains in the E-cast film results in greatly increased global mobility. Notably, the existence of large-scale layered structures in spin-cast films implies that charge-carrier mobility can be *highly anisotropic*. Thus, the mobility difference between a spin-cast diode and a field-effect transistor, in addition to the carrier-density effect,[23] may be because of morphological differences.

## 5. Experimental

### 5.1. Sample Preparation

Following generally the procedure reported by Wudl and co-workers [24,25], MEH-PPV of weight-average molecular mass $M_w \approx 250$ kD, polydispersity 6.5 (determined via gel-permeation chromatography), and tetrahedral defect density of ca. 2 % (determined by NMR) was synthesized via the Gilch method. The resulting polymer MEH-PPV was dissolved for several weeks in chlorobenzene (5 mg mL$^{-1}$). Solutions were kept in a dark room under an inert $N_2$ atmosphere until film casting was performed on pre-cleaned ITO glass substrates.

Films were prepared by spin-casting, drop-casting, or drop-casting in the presence of an electric field [16,18,19]. The thicknesses of the films were measured using a Dektak 3030 surface profiler and were generally of the order of 30 nm for spin-cast films and 4 μm for two types of drop-cast films. Figure 11 gives cross-sectional views of the experimental setup for the application of the electric field during drop-casting and the electric-field distribution around and within the MEH-PPV film as simulated using Maxwell 2D-SV software (Ansoft Corporation). The grounded stainless steel electrode was in electrical contact with the ITO substrate by use of a Ag paste. A 5 mm air gap separated the high-voltage (HV) electrode (3.5 kV) from the ITO. In the simulation, electrodes were taken as stainless steel, the ITO layer assumed to be a perfect conductor sitting on an insulating glass substrate, and MEH-PPV was taken as being dielectric.

### 5.2. Sample Characterization

Films were checked for uniformity by use of scanning confocal microscopy (SCM) and atomic force microscopy (AFM). The SCM was made in-house. AFM measurements were performed using a PSIA XE-100 instrument making use of non-contact high-resonance frequency (NCH) type cantilevers with Al reflection coating (Nanosensors). All measurements were made under ambient conditions in a non-contact dynamic mode where the detection frequency exceeds resonance, in contrast to the standard tapping mode. By detecting changes in lock-in amplitude (or phase), the surface can be imaged without noticeable reduction of the actual cantilever vibration amplitude. This reduces wear and damage to the soft specimens used in this study.

### 5.3. Optical Spectroscopy

As self-absorption is a factor that can affect the measured optical properties of thin films, three different methods of optical spectroscopy were used. As PL is particularly sensitive to self-absorption, both PL and PLE spectra were collected in the front-face geometry to minimize the effects from self-absorption. This was checked using a range of concentrations of rhodamine 610 dissolved in ethanol (optical density OD = 0.016 to 1.6): the PL spectra exhibited a small difference (< 5 %, see Fig. S1). Both spectra were recorded by a Jobin Yvon FL3–21 spectrofluorometer.

Fluorescence decay curves were recorded using a femtosecond mode-locked tunable Ti:sapphire laser (Coherent, Mira 900 operating at $\lambda = 920$ nm) passed through a second harmonic generator to generate the 460 nm excitation light source. Fluorescence was passed through a monochromator (Acton SP-150) and measured with a streak camera (Hamamatsu C5680-01). The overall time resolution of the instrument was better than 5 ps.

### 5.4. Charge mobility

The device capacitance was measured by a Hewlett Packard 419A impedance/gain phase analyzer and found to be 30 and 300 pF for the thick and thin film devices, respectively. Room-temperature charge-transport characteristics were measured by the time-of-flight (TOF) technique for thick-film devices and transient electroluminescence (TrEL) [26] for thin-film devices. Both TOF and TrEL signals were recorded by a digital-storage oscilloscope (Tektronix TDS 744 A).

For TOF measurements, an Al electrode (2 mm × 2 mm) was deposited by thermal evaporation/shadow-masking to form a diode structure. The transit time ($t_{tr}$) was determined from the characteristic break in


© 2007 WILEY-VCH Verlag GmbH & Co. KGaA, Weinheim

ADVANCED FUNCTIONAL MATERIALS



the logarithmic current–time plot. The drift mobility ($\mu_d\Delta$) was calculated as

$$\mu_d = L/t_{tr}E \quad (1)$$

where $L$ is the device thickness and $E$ the applied electric field. In TOF experiments, one concern is the space-charge effects. In general, space-charge effects are minimal if the injected charge $\ll CV$ where $C$ is the structure capacitance (ca. 30 pF in our devices) and $V$ is the applied voltage (40 V in our case). To avoid space-charge effects, the total charge injected into the film was ca. 100 pC [18,19,27]. We note that dispersiveness of the TOF signal not only depends on the optical quality of the samples, but also on the energy and position disorder within the samples, as demonstrated in the case of MEH-PPV films prepared from chlorobenzene and toluene [19,27]. Despite identical optical spectra, the films spun from the first solvent were found to exhibit dispersive mobility whereas those from the second were non-dispersive. Temperature-dependent and structural studies revealed that the morphological factors responsible for energy and positional disorders determine the quality of TOF transients.

For TrEL measurements the films were placed in an inert atmosphere for 6 h. The remaining solvent, along with any adsorbed oxygen, was removed by storing the samples in high vacuum for another 12 h. During the entire specimen preparation process, the solution or film temperatures were never raised above ambient temperature. An Al electrode (0.5 $mm^2$) was deposited onto the MEH-PPV film via thermal evaporation and shadow masking. Devices were placed in a cryostat under dynamic high vacuum of $1 \times 10^{-6}$ Torr for 12 h prior to the TrEL measurements carried out in the same dynamic vacuum. Electrical excitations were achieved by rectangular electrical pulses generated by a home-made pulse generator (10 ns in rise time, 10 Hz in frequency, variable pulse width up to 60 μs). Electroluminescence (EL) was detected by a photomultiplier (Hamamatsu R955) placed on top of the glass window of the cryostat. For a similar OLED device, the depletion region was found to be ca. 100 nm on the basis of capacitance–voltage analysis [13,28], indicating that the field strength across the MEH-PPV layer is uniform in the 30 nm devices investigated here. Under these conditions, the delay time between the rising edge of the applied voltage and the onset of EL is approximately equal to the transit time for the charge carriers to travel across the device, allowing mobility to be determined using Equation 1. We note that the $RC$ time constant of the TrEL set-up (0.1 μs) was much shorter than the delay time.

Although hole mobility generally exceeds electron mobility in MEH-PPV films by two orders of magnitude [29], it is possible to observe electron-dominated charge transport in phenyl-substituted poly(phenylenevinylene)s using TOF with appropriate biasing. For example, in a single-layer MEH-PPV device, one can switch from hole-dominance to electron-dominance by simply changing the electrode configuration from Au/MEH-PPV/Al to TiN/MEH-PPV/Ca/Al [30]. Nevertheless, for the device structure ITO/MEH-PPV/Al used here in both TOF and TrEL measurements, the injection of electrons from the cathode is suppressed because of the ca. 1.3 eV barrier between the aluminum electrode (work function $\Psi = 4.2$ to 4.3 eV) and the MEH-PPV film (LUMO energy ranges from 2.8 to 3.0 eV) [31–33]. Thus, in both TrEL and TOF configurations the charge transport is hole-dominated.

### 5.5. Film Morphology

The film morphology was studied by means of X-ray reflectivity (XRR) and field-emission scanning electron microscopy (FESEM). For XRR measurements, films were cast on 50 mm × 20 mm (length by width) substrates. Profiles of spin-cast (on quartz plate), drop-cast (on quartz plate), and E-cast (on ITO glass plate) films were first measured using an in-house X-ray source and repeated using the synchrotron radiation source of the wiggler beamline BL17B1 in the National Synchrotron Radiation Research Center (NSRRC) for high-quality data. For the latter measurements, two pairs of slits were used to collimate a monochromatic beam of 8 keV photons (wavelength $\lambda = 1.55$ Å) with a beam size of 1.0 mm × 0.2 mm (width by height) at the sample position. Two additional slit sets of the same openings as the beam dimensions at the sample position were positioned, respectively, behind the sample and in front of the NaI scintillation counter. The sample-to-detector distance was 1 meter. The setup provided a $Q$-resolution of 0.0008 $Å^{-1}$ in the reflectivity measurement, where $Q = 4\pi\sin\theta/\lambda$ (with $\theta$ the incident angle is the X-ray wave-vector transfer perpendicular to the sample surface. Reflectivity data were obtained in the $Q$-range of 0.005 to 0.33 $Å^{-1}$.

The X-ray reflectivity as a function of $Q$ provides information about the in-depth density profile of a film [34]. For a homogeneous film, the reflectivity follows the Fresnel formula. For a layered structure, the Fresnel reflectivity will be modulated by additional interference from layers inside the film. For sufficiently flat and sufficiently thin films, the reflection from the top surface interferes with the reflection from the bottom interface (film–substrate) resulting in constructive interference, or Kiessig fringes. From the periodicity ($\Delta Q'$) of these fringes, the film thicknesses of the spin-cast films were obtained with very high accuracy ($t = \Delta Q'/2\pi$). Modulation of the fringes indicates additional layering within the film, with the period of modulation inversely proportional to the layer thickness.

In order to quantitatively extract the in-depth density profile of the drop-cast film from the reflectivity data (Figs. S2 and S3), a standard model fitting algorithm for multilayer structures was used in which a continuous transition between successive layers of different density $\rho$ or scattering length density, $\rho b$ (with $b$ the molecular scattering length), is accounted for by an effective Debye–Waller factor. The beam absorption upon traversing the film was taken into account in the fitting algorithm using the density and X-ray linear absorption $\mu$ of the film calculated from the total reflection wave vector $Q_c$ (reflectivity = 1) observed [19].

Topographic features of cryogenically fractured surfaces of as-cast and E-cast MEH-PPV films (floated off from the substrate using a dilute HF solution) were examined via secondary-electron images obtained by use of a field-emission scanning electron microscope (JEOL JSM-6330TF) under an accelerating voltage of 10 kV. To avoid charging, specimens were sputter-coated with a thin layer of gold prior to SEM observations.

### 5.6. Appendix

Finally we address the issue of film thickness, which is also an important factor in charge-mobility measurements. While the drop-cast and E-cast devices operate in the non-dispersive region, the spin-cast devices operate in the dispersive region. In the dispersive region, mobility scales weakly with thickness. According to the model of Scher and Montroll [35] (SM), transit time and mobility in this dispersive region scales with thickness according to [36]

$$t_{tr}^{-1} \propto (E/L)^{1/\alpha} \quad (2)$$

and

$$\mu \propto (E/L)^{1/\alpha - 1} \quad (3)$$

where $E$ is the electric field, $L$ is the film thickness and $0 \le \alpha \le 1$. The value of $\alpha$ is determined from the slope of the transient current in the logarithmic plot. In Figure 12, the inverse transit time for the three films is plotted against $E/L$. Interestingly, although the SM model is strictly applicable to only the spin-cast film, the field-dependent inverse transit times lie along a line having a slope in reasonable agreement with the SM model for all three types of devices. Nevertheless, the plots do not follow the same line, indicating that the observed mobility differences between the films are not merely a result of dispersive transport in films of different thickness. Furthermore, the SM scaling law dictates decreases in apparent mobility with increasing film thickness but an opposite trend is observed in going from spin-cast to drop-cast devices. Altogether, these observations suggest that the low mobility in


© 2007 WILEY-VCH Verlag GmbH & Co. KGaA, Weinheim

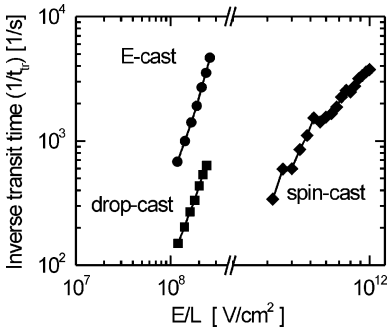


**Figure 12.** Comparison of reciprocal transit times ($1/t_{tr}$) plotted against $E/L$ at room temperature for drop-cast, E-cast, and spin-cast devices. (See Eq. 2 in the text for details.) The slopes for the drop-cast, E-cast, and spin-cast devices were $2.1 \times 0.2$, $2.4 \times 0.2$, and $2.0 \times 0.2$ (low-field side), respectively.

the spin-cast device is not an artifact due to the thickness-dependent dispersion effects but more likely related to inherent differences in the MEH-PPV film morphology among the different devices.

Received: September 8, 2006
Revised: March 19, 2007
Published online: August 28, 2007

[1] *Organic Photoreceptors for Imaging Systems* (Eds: P. M. Borsenberger, D. S. Weiss) Marcel Dekker, New York, NJ **1998**.
[2] R. H. Friend, R. W. Gymer, A. B. Holmes, J. H. Burroughes, R. N. Marks, C. Taliani, D. D. C. Bradley, D. A. Dos Santos, J. L. Brédas, M. Løgdlund, W. R. Salaneck, *Nature* **1999**, *397*, 121.
[3] *Electronic Processes in Organic Crystals and Polymers* (Eds: M. Pope, C. E. Swenberg), Oxford University Press, Oxford, UK **1999**.
[4] D. D. C. Bradley, M. Grell, A. Grice, A. R. Tajbakhsh, D. F. O'Brien, A. Bleyer, *Opt. Mater.* **1998**, *9*, 1.
[5] B. J. Schwartz, *Annu. Rev. Phys. Chem.* **2003**, *54*, 141.
[6] J. Liu, Y. J. Shi, L. P. Ma, Y. Yang, *J. Appl. Phys.* **2000**, *88*, 605.
[7] T. Q. Nguyen, R. C. Kwong, M. E. Thompson, B. J. Schwartz, *Synth. Met.* **2001**, *119*, 523.
[8] T. Q. Nguyen, I. B. Martini, J. Liu, B. J. Schwartz, *J. Phys. Chem. B* **2000**, *104*, 237.
[9] T. L. Lim, C. W. Chang, A. R. Inigo, Y. F. Huang, J. D. White, W. Fann, *Chem. Phys. Lett.* **2006**, *432*, 564.
[10] T. Q. Nguyen, V. Doan, B. J. Schwartz, *J. Chem. Phys.* **1999**, *110*, 4068.
[11] Y. Shi, J. Liu, Y. Yang, *J. Appl. Phys.* **2000**, *87*, 4254.
[12] S. H. Chen, A. C. Su, Y. F. Huang, C. H. Su, G. Y. Peng, S. A. Chen, *Macromolecules* **2002**, *35*, 4229.
[13] S. A. Arnautov, E. M. Nechvolodova, A. A. Bakulin, S. G. Elizarov, A. N. Khodarev, D. S. Martyanov, D. Y. Paraschuk, *Synth. Met.* **2004**, *147*, 287.
[14] V. R. Nikitenko, H. Bässler, *J. Appl. Phys.* **2000**, *88*, 1886.
[15] C. Im, H. Bässler, H. Rost, H. H. Horhold, *J. Chem. Phys.* **2000**, *113*, 3802.
[16] U. Jeng, C. H. Hsu, H. S. Sheu, H. Y. Lee, A. R. Inigo, H. C. Chiu, W. S. Fann, S. H. Chen, A. C. Su, T. L. Lin, K. Y. Peng, S. A. Chen, *Macromolecules* **2005**, *38*, 6566.
[17] C. Y. Yang, F. Hide, M. A. Diaz-Garcia, A. J. Heeger, Y. Cao, *Polymer* **1998**, *39*, 2299.
[18] A. R. Inigo, C. C. Chang, W. Fann, J. D. White, Y. S. Huang, U. S. Jeng, H. S. Sheu, K. Y. Peng, S. A. Chen, *Adv. Mater.* **2005**, *17*, 1835.
[19] A. R. Inigo, H. C. Chiu, W. Fann, Y. S. Huang, U. S. Jeng, T. L. Lin, C. H. Hsu, K. Y. Peng, S. A. Chen, *Phys. Rev. B* **2004**, *69*, 075 201.
[20] A similar layer-like structure has been reported to exist *within* the local ordered domains of drop-cast films: S. H. Chen, A. C. Su, S. R. Han, S. A. Chen, Y. Z. Lee, *Macromolecules* **2004**, *37*, 181.
[21] P. W. M. Blom, C. Tanase, D. M. de Leeuw, R. Coehoorn, *Appl. Phys. Lett.* **2005**, *86*, 092 105.
[22] Q. M. Shi, Y. B. Hou, J. Lu, H. Jin, Y. B. Li, Y. Li, X. Sun, J. Liu, *Chem. Phys. Lett.* **2006**, *425*, 353.
[23] C. Tanase, E. J. Meijer, P. W. M. Blom, D. M. de Leeuw, *Phys. Rev. Lett.* **2003**, *91*, 216 601.
[24] F. Wudl, G. Srdanov, *US Patent 5 189 136*, **1990**.
[25] F. Wudl, G. Srdanov, *Chem. Abstr.* **1993**, *118*, 255 575.
[26] S. Karg, V. Dyakonov, M. Meier, W. Riess, G. Paasch, *Synth. Met.* **1994**, *67*, 165.
[27] A. R. Inigo, C. H. Tan, W. Fann, Y. S. Huang, G. Y. Perng, S. A. Chen, *Adv. Mater.* **2001**, *13*, 504.
[28] S. Karg, W. Riess, V. Dyakonov, M. Schwoerer, *Synth. Met.* **1993**, *54*, 427.
[29] L. Bozano, S. A. Carter, J. C. Scott, G. G. Malliaras, P. J. Brock, *Appl. Phys. Lett.* **1999**, *74*, 1132.
[30] J. C. Scott, P. J. Brock, J. R. Salem, S. Ramos, G. G. Malliaras, S. A. Carter, L. Bozano, *Synth. Met.* **2000**, *111*, 289.
[31] I. D. Parker, *J. Appl. Phys.* **1994**, *75*, 1656.
[32] I. H. Campbell, T. W. Hagler, D. L. Smith, J. P. Ferraris, *Phys. Rev. Lett.* **1996**, *76*, 1900.
[33] S. H. Jin, M. S. Jang, H. S. Suh, H. N. Cho, J. H. Lee, Y. S. Gal, *Chem. Mater.* **2002**, *14*, 643.
[34] L. G. Parratt, *Phys. Rev.* **1954**, *95*, 359.
[35] H. Scher, E. W. Montroll, *Phys. Rev. B* **1975**, *12*, 2455.
[36] G. Pfister, H. Scher, *Adv. Phys.* **1978**, *27*, 747.


© 2007 WILEY-VCH Verlag GmbH & Co. KGaA, Weinheim